Afyon Kocatepe Üniversitesi Fen ve Mühendislik Bilimleri Dergisi

Afyon Kocatepe University Journal of Science and Engineering

AKÜ FEMÜBİD **22** (2022) 061101 (1256-1270) AKU J. Sci. Eng. **22** (2022) 061101 (1256-1270)

DOI: 10.35414/ akufemubid.1143137

Araştırma Makalesi / Research Article

Investigation of the Cross Sections and Effect of Level Density Models for Platinum Element in the Production of $^{191-199}$Au Medical Isotopes

Nurdan KARPUZ DEMİR[1]

[1]*Amasya Üniversitesi, Sabuncuoğlu Şerefeddin Sağlık Hizmetleri Meslek Yüksekokulu, Tıbbi Hizmetler ve Teknikler Bölümü, Amasya.*

Sorumlu yazar e-posta: nurdankarpuz@amasya.edu.tr ORCID ID: http://orcid.org/0000-0003-4911-8846

Geliş Tarihi: 11.07.2022 Kabul Tarihi: 23.11.2022

Keywords
Production cross section; Platinum target; Deuteron induced reactions; Level density models; $^{191-199}$Au Medical radioisotope

Abstract

In cases where experimental studies cannot be carried out and there is no experimental data with it, studies carried out with theoretical models shed light on the researchers' knowledge of different data. The most important of this data is the measurable or calculatable influence cross-section value, which is defined as the probability of a reaction occurrence. Examining the possible effects of different models in the calculation of the effect section is important for the correct calculation of this value. The most important data, the cross section of influence, has taken its place in the radioisotope world on the side in many fields of nuclear physics. With developing technology and advancing science, radioisotopes have widespread and diversified uses. Most commonly, radioisotopes are used in medical diagnosis and treatment applications. Among the many radioisotopes used for this purpose, $^{191-199}$Au radioisotopes are also important in terms of both their benefits and characteristics in medical applications. In this respect, the study aimed to analyze the influences of different nuclear level density models in production impact cross-section calculations of $^{191-199}$Au radioisotopes with deuteron reference. Theoretical cross sections using the TALYS code have been simulated for all isotopes. The results of the calculations obtained were compared with each other and with the experimental data in the literature and it was aimed to define the most compatible level density models according to the reaction situations examined.

Platinyum Element İçin $^{191-199}$Au Medikal İzotop Üretim Tesir Kesitlerinin ve Seviye Yoğunluk Modellerinin Etkisinin İncelenmesi

Anahtar kelimeler
Üretim tesir kesiti; Platinyum hedef; Döteron indüklenmiş reaksiyonlar; Seviye yoğunluk modelleri; $^{191-199}$Au Medikal radyoizotop

Öz

Deneysel çalışmaların yapılamadığı ve bununla birlikte deneysel verilerin bulunmadığı durumlarda, teorik modellerle yapılan çalışmalar, araştırmacıların farklı veriler hakkındaki bilgilerine ışık tutmaktadır. Bu verilerden en önemlisi, bir reaksiyonun oluşma olasılığı olarak tanımlanan ölçülebilir veya hesaplanabilir tesir kesiti değeridir. Tesir kesiti bölümünün hesaplanmasında farklı modellerin olası etkilerinin incelenmesi, bu değerin doğru hesaplanması açısından önemlidir. En önemli veri olan tesir kesiti, radyoizotop dünyasında olduğu gibi nükleer fiziğin birçok alanında da yerini almıştır. Gelişen teknoloji ve ilerleyen bilim ile radyoizotopların yaygın ve çeşitli kullanımları vardır. En yaygın olarak radyoizotoplar medikal tanı ve tedavi uygulamalarında kullanılmaktadır. Bu amaçla kullanılan birçok radyoizotop arasında $^{191-199}$Au radyoizotopları da tıbbi uygulamalarda hem yararları hem de özellikleri açısından önemlidir. Bu bağlamda çalışmada, $^{191-199}$Au radyoizotoplarının üretim tesir kesit hesaplamalarında farklı nükleer seviye yoğunluk modellerinin etkilerinin döteron referansı ile araştırılması amaçlanmıştır. TALYS kodunun kullanıldığı teorik kesitler tüm izotoplar için simüle edilmiştir. Elde edilen hesaplamaların sonuçları birbirleri ve literatürdeki deneysel verilerle

karşılaştırılmış ve incelenen reaksiyon durumlarına göre en uyumlu seviye yoğunluk modellerinin belirlenmesi amaçlanmıştır.

1. Introduction

Nuclear reaction is said to occur when a nuclear particle comes into close contact with another particle. During interaction, an exchange of energy and momentum are characterized by the incoming nuclei and the outgoing reaction products (Asres *et al*. 2019). The cross section is an important quantity in studying the nuclear reaction, where it helps to calculate the probability of nuclear reaction, therefore, it became the main concern since the beginning of nuclear reaction studies (Abdullah *et al*. 2020). The cross section is a mathematical version of describing the probability of a nuclear reaction occurring. The cross-sectional value of a reaction can be expressed as the value that clearly indicates the probability of that reaction occurring. This value can be measured with the help of experimental studies.

The use of systematics for nuclear reaction cross section evaluation is important, if experimental data are absent or results of nuclear model calculation are not reliable. Systematics of cross sections has a special importance as an additional tool for the cross section evaluation (Tel *et al*. 2016). Studies of excitation functions of nuclear reactions are of considerable importance for testing nuclear models as well as for practical applications (Sudar *et al*. 2006). Theoretical nuclear models are very important in terms of guiding researchers in the lack of experimental cross section data. The development of a model compatible with experimental datum is of great significance for solving fundamental nuclear physics problems (Lilley, 2018). Thanks to the reaction models in the nuclear codes, it is possible to predict the shapes of the nuclear sections. Consequently, these reaction and level density types are required to make predictions about excitation functions. Nuclear reaction models and nuclear effect keywords for the decay of compound nuclei are a convenient way to estimate and evaluate yields for dissimilar reactions. These codes are very important in cross section calculations in a extensive range of incident energy. In addition, one of the most significant inputs in reaction cross section computation is the nuclear level density. According to literature, energy level density can be described as the number of nuclear energy levels per MeV. To learn the density of the nuclear levels at different excitation energies, in the calculation of the sudden neutron spectra resulting from different nuclear reactions and fission, in the determination and classification of the energy level density, which is an important subject of nuclear spectroscopy; It has an important place in making statistical calculations in fission-fusion reactor physics, astrophysics and heavy ion collision studies.

Experiments with targets of a natural isotope composition provide necessary information about the interaction mechanism specific, on the whole, for a given element and do not allow investigations into particular reaction channels dependent on the nucleon composition of the interacting nuclei (Kulko *et al*. 2012).

Investigations of excitation functions of nuclear effects are of significant emphasis for testing nuclear models on the side for convenient utilizations. It should be noted that dissimilar nuclear reaction sections consist of with dissimilar possibilities. Physically, the possibility of a reaction is described in an amount called a nuclear cross section. The forms of nuclear cross sections can be estimated using reaction types in nuclear codes. As a result, these types are requiremented to provide trained estimates of excitation functions. Nuclear reaction codes for the degradation of the compound nucleus are an advantage way to guess and evaluate yield for dissimilar reactions.

There are experimental (Vagena and Stoulos 2017), (Stoulos and Vagena, 2018), (Ghergherehchi *et al*. 2012), (Hu *et al*. 2022), (Sziki *et al*. 2006), (Usman *et*

al. 2016), (Usman *et al*. 2017), (Usman *et al*. 2016), (Usman *et al*. 2020) and theoretical (Kaplan *et al*. 2014), (Aydın *et al*. 2015), (Kaplan *et al*. 2015), (Özdoğan *et al*. 2018), (Artun 2018), (Artun 2019), (Sarpün *et al*. 2019), (Canbula *et al*. 2014), (Canbula 2020), (Noori *et al*. 2019), (Noori *et al*. 2017), (Demir 2017), (Noori *et al*. 2016), (Karpuz 2016), (Noori *et al*. 2018), (Kavun and Makwana 2021), (Kavun *et al*. 2020), (Kavun and Makwana 2020) nuclear reaction section studies in the literature that conducted in the light of this direction.

The deuteron induced reactions play an important role in the accelerator based high intensity neutron sources (d-Be, d-Li). These high intensity neutron sources have broad applications in development of the fusion technology, in boron neutron capture therapy, in accelerator based transmutation systems, etc. Although platinum is not a basic material for nuclear technology, it is an important component of alloys or minor small parts used in several electronic devices, collimators, thermometers, target backings, etc (Tarkanyi *et al*. 2004).

Light ion-sending activation effects to platinum are important in different areas such as model computations, accelerator technology, loaded particle activation analysis, medical isotope production. The results in natural elements are useful for the use of radioisotope in medicine for the production of related radioisotope, as well as for estimation of the need for the description of nuclear datum.

In this study, the cross section values of the ^{nat}Pt deuteron-induced reaction were computed using different nuclear level density models. Calculations were performed with version 1.95 of the TALYS nuclear code (Koning *et al*. 2019). The calculation results obtained and the experimental data of the reaction obtained from the experimental database were compared. The details of the level density models used for the calculations are presented in the Material and Method section, and the results are presented in the Results and Discussions section.

2. Material and Method

In different practical applications often either the knowledge of the total produced activity or the distribution of that activity as a function of depth, bombarding energy and the target thickness are more convenient to use than the microscopic cross-section data. The production yield is directly connected to the cross-section and to the composition of the used target (Tarkanyi *et al*. 2004).

Nuclear reaction calculations require complete and clearly defined nuclear level densities (Koning *et al*. 2008). The level density is the number of levels per unit energy at a certain energy. So, the level density model is important input parameter in the cross section calculations. Namely, the level density has been investigated through applications such as astrophysics, fission, fusion and radionuclide production (Yiğit *et al*. 2016), (Yiğit *et al*. 2017).

Nuclear-level density models are valid in the literature. TALYS has six level density models relating to two groups, phenomenologically and microscopically. Level density models that are phenomenological are Constant Temperature Fermi Gas Model (CT + FGM) (Gilbert and Cameron 1965)**,** Back-shifted Fermi Gas Model (BSFGM) (Bethe 1937), (Dilg *et al*. 1973) and Generalized Superfluid Model (GSM) (Ignatyuk *et al*. 1979), (Ignatyuk *et al*. 1993). The three microscopic level density models found in Talys are Skyrme Force-Goriely (SFG) (Goriely *et al*. 2001), Skyrme Force-Hilaire (SFH) (Goriely *et al*. 2008) and temperature-dependent Hartree-Fock-Bogoliubov Gogny Force (Hilaire *et al*. 2012).

Most commonly used level density models are relating to the Fermi Gas Model (Bethe 1937), which assumes the single-particle state in which the excited levels of the nucleus are evenly spaced and there are no collective levels. The first level density model developed is the Fermi Gas Model introduced by Bethe (Bethe 1937). This model is relating to the supposition of single particle state, in which the stimulated levels of the nucleus are evenly spaced and there are no collective levels. Nucleons do not interact with each other, they are located in equal spaces at one-particle energy levels, and they do not have collective levels. According to the Fermi Gas Level density model, protons and neutrons occupy

the lowest energy levels. Although this fundamental assumption supports the Fermi gas model for low energies to yield successful results; failed results at much higher energies. In the Constant Temperature Model, a constant temperature rule is applied for the energy zone in the portion from 0 MeV to a match energy. Correspondingly, greater energy value than match energy is applied to Fermi Gas Model (FGM). The state in the Back-shifted Fermi Gas Model (BSFGM) is that at high energies, the excitation energy of the Fermi gas expression includes a shifting parameter. In the Generalized Superfluid Model (GSM), superconducting mating correlations are active. And accordingly, according to Bardeen-Cooper-Schrieffer theory, computational syntax is the case analysis of a phase transition from low-energy superfluid behavior to a high-energy zone described by the Fermi gas model, where mating correlations show a strong effect on level density. Hartree-Fock-based microscopic level density models demonstrate close success to phenomenological models in retrieving experimental data and adapting it to nuclear applications.

TALYS Computer Programme

TALYS, is one of the widely used computer programs for the cross-section computations of nuclear reactions. It is a program that can simulate nuclear reactions involving protons, neutrons, deuterones, tritons, alpha particles, and gamma rays in the energy range of 1 keV to 1 GeV. TALYS is preferred in both basic and applied sciences. It is written in Fortran 77 programming language. Over time, continuous updates were made to eliminate the deficiencies seen on TALYS. In this study, dissimilar nuclear level intensity models were calculated using the latest version of TALYS.

3. Results and Discussions

The cross section of platinum is very available in the production of medical radioisotopes, in the classification of nuclear reaction theory, in thin layer activation analysis. In this study, the impact section values of ^{nat}Pt, which is one of the transition metals that are important with its different practices in science and technology, and the production impact section calculations of $^{191-199}$Au radioisotopes were calculated with TALYS 1.95 computer program (Koning *et al*. 2019) using nuclear level density models. To research productions of Au radioisotopes by level density models, i.e., Constant Temperature Fermi gas model (CTM), Back-shifted Fermi gas model (BFM), Generalised Superfluid Model (GSM), Skyrme-Hartree-Fock-Bogoluybov level densities from numerical tables (SHFBM), Gogny-Hartree-Fock-Bogoluybov level densities from numerical tables (GHFBM), Temperature-dependent Gogny-Hartree-Fock-Bogoluybov level densities from numerical tables (TGHFM), are calculated the cross sections. Moreover, the yields and the cumulative number of levels of effect for the level density models are calculated. Comparison of all theoretical calculated results obtained from the models with both each other and with the experimental datum, valid in the EXFOR (Int Kyn. 1) database in literature. Figures 1-8 represent calculated cross section effects with the all of level density models for ^{nat}Pt(d,x)$^{191-199}$Au, respectively. The yields of the production alpha, deuteron, helium-3, neutron, proton and triton are calculated and are indicated on the figure (Figure 9-14). And the cumulative number of levels values (Figure 15-19) are indicated on the figure. The relative variance analysis of reaction calculations for radionuclides of gold are also presented in tabular (Table 1).

3.1. Production cross sections for radionuclides of gold

3.1.1 ^{nat}Pt(d,x)^{191}Au reaction

The computation cross section results with six level density models, (CTM), (BFM), (GSM), (SHFBM), (GHFBM), (TGHFM), for the radionuclides of ^{191}Au are indicated in Fig. 1 and the relative variance analysis of reaction cross section calculations in Table 1. These calculated results are checked against with the experimental results in the literature (Tarkanyi *et al*. 2019), (Ditroi *et al*. 2017), (Ditroi *et al*. 2006). The level density model results are harmonious with each other up to 60 MeV. The model computations are in harmonious with the experimental results in 38 MeV. For this reaction, value of maximum calculated cross section is 50,5

MeV. The experimental cross section results are convenient to the conclusion of GSM in the area between 28 MeV and 55 MeV.

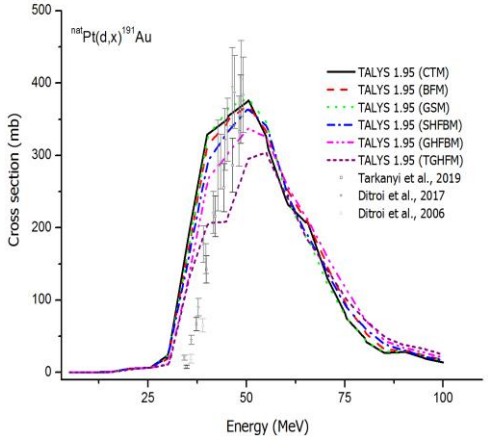

Fig. 1. Calculated cross section for $^{nat}Pt(d,x)^{191}Au$ reaction.

3.1.2 $^{nat}Pt(d,x)^{192}Au$ reaction

The nuclear cross sections for $^{nat}Pt(d,x)^{192}Au$ reaction in energy range 5-100 MeV are shown in Fig. 2. In Fig. 2, the cross section graph for the (d,x) reaction is demonstrated as derived by the six level density models and efficiently together with experimental data (Tarkanyi *et al*. 2019), (Tarkanyi *et al*. 2004), (Khandaker *et al*. 2015), (Ditroi *et al*. 2017) and (Ditroi *et al*. 2006). The model calculations match to each other. It is explicit that the maximum of the calculated cross section graph for the radionuclide of ^{192}Au occurs at 35 MeV. Up to the maximum of theoretical excitation curve, there are differences between the theoretical and experimental results.

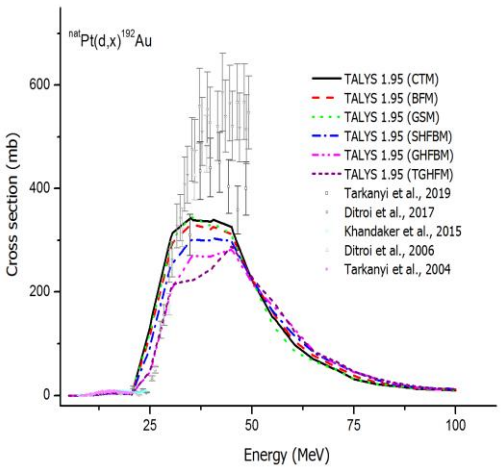

Fig. 2. Calculated theoretical cross section for $^{nat}Pt(d,x)^{192}Au$ reaction.

3.1.3 $^{nat}Pt(d,x)^{193}Au$ reaction

For production of ^{193}Au, the nuclear reaction cross sections are shown in figure 3. Figure 3 is indicated in conjunction with experimental data from EXFOR, the reaction cross-section curve and six-level density model of the reaction for the production of $^{193}Au(d,x)$. The calculated cross sections of ^{193}Au show a consisteny with the experimental measurements by (Tarkanyi *et al*. 2019), (Tarkanyi *et al*. 2004), (Ditroi *et al*. 2017), (Ditroi *et al*. 2006) and (Khandaker *et al*. 2015). Although the cross section of ^{193}Au is considerable, the contribution of SHFBM, GHFBM and TGHFM level density model of ^{193}Au reaction was found to be insignificant small.

Level density models are checked against with each other. As an energy value of 54 MeV, experimental data are harmonious with level density models. The calculated maximum cross section amount for this reaction is in the GHFBM level density model at 30 MeV. When the level density models are checked against with each other, the maximum impact cross section value is 30 MeV, although it is the same in all of them.

Table 1 Analysis of variance for production cross section calculations of the $^{191,192,193,194,195,196,198,199}Au$ radionuclides by using level density models

Isotope	CTM	BFM	GSM	SHFBM	GHFBM	TGHFM

^{191}Au	177033	173100	18222	16180	14422	10320
^{192}Au	15494	14072	14740	11934	9928	9174
^{193}Au	19502	20308	20816	23562	26076	24230
^{194}Au	15481	12407	11343	8893	14244	14164
^{195}Au	6666	7478	7248	10635	8211	7572
^{196}Au	835	932	820	1064	1149	1130
^{198}Au	24	31	30	50	46	46
^{199}Au	0,042	0,064	0,049	0,076	0,060	0,101

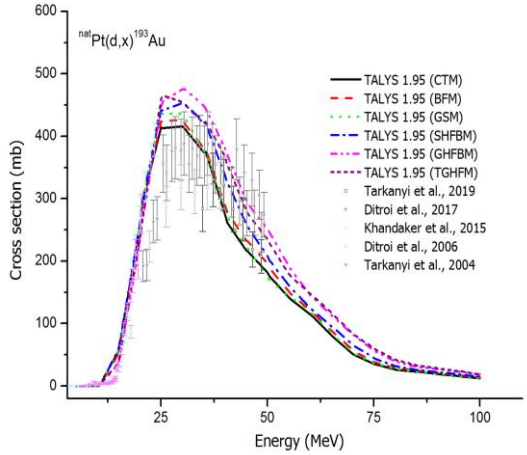

Fig. 3. Calculated cross section for ^{nat}Pt(d,x)^{193}Au reaction.

3.1.4 ^{nat}Pt(d,x)^{194}Au reaction

The relative variance analysis production of ^{194}Au is due to the contributions from the six level density models listed in Table 1. The calculated excitation function of ^{194}Au is shown in Fig. 4 together with experimental data (Tarkanyi *et al*. 2019), (Tarkanyi *et al*. 2004), (Khandaker *et al*. 2015), (Ditroi *et al*. 2017), (Ditroi *et al*. 2006) and (Kulko *et al*. 2012) from EXFOR. The cross sections reported by Tarkanyi *et al*., Ditroi *et al*., Khandaket *et al*. and Kulko *et al*. are clearly discrepant with the calculated results. Based on the calculated cross section values and the experimental cross section values, although there is a discrepancy in the numerical data, the formal representation as the cross section curve is in harmony with each other. The level density model consequences are harmonious with each other up to 55 MeV. The model calculations are in agreement with the experimental results in 20 MeV. The maximum calculated cross section amount of this reaction is 25,5 MeV. The experimental conclusions are convenient to the result of GSM in the area between 5 MeV and 25 MeV.

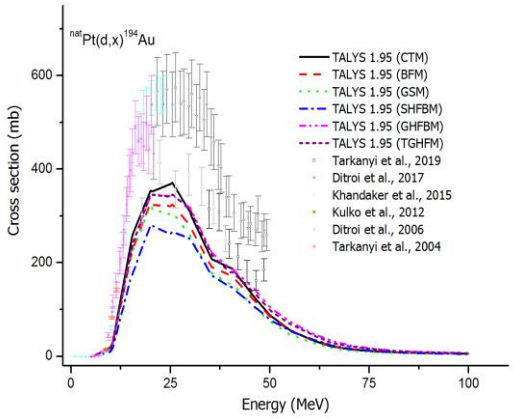

Fig. 4. Calculated cross section for ^{nat}Pt(d,x)^{194}Au reaction.

3.1.5 ^{nat}Pt(d,x)^{195}Au reaction

The relative variance analysis of ^{195}Au radioisotope production reaction effect cross section data where level intensity models were examined are indicated in Table 1. The calculated cross sections of ^{195}Au are plotted in Fig. 5. The experimental cross sections reported by (Khandaker *et al*. 2015), (Kulko *et al*. 2012), (Ditroi *et al*. 2006) and (Ditroi *et al*. 2017) show only a partial agreement with the calculated results. Tarkanyi *et al*. (2004 and 2019) reported the ^{nat}Pt(d,x)^{195}Au cross sections in the energy area of 6.9-20.3 MeV and 34.8-48.5 MeV, and they showed a good agreement with the calculated results. The level density model conclusions are harmonious with each other up to 20 MeV. The model calculations are in harmony with the experimental conclusions in 15 MeV. The maximum calculated cross section amount of this reaction is 20 MeV. The experimental conclusions are close to the result of SHFBM in the area between 6 MeV and 15 MeV.

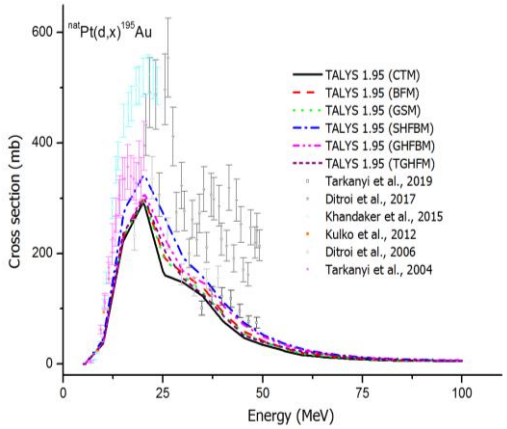

Fig. 5. Calculated cross section for $^{nat}Pt(d,x)^{195}Au$ reaction.

3.1.6 $^{nat}Pt(d,x)^{196}Au$ reaction

The calculated excitation functions of ^{196}Au and effect of level density models are displayed in Fig. 6 together with the experimental data from the EXFOR library. The production of ^{196}Au is due to the contributions from the six level density models with variance analysis listed in Table 1. Calculated values with experimental results are formally compatible. The calculated cross sections of ^{196}Au show a consisteny with the experimental measurements by (Tarkanyi *et al*. 2019), (Tarkanyi *et al*. 2004), (Ditroi *et al*. 2017), (Ditroi *et al*. 2006), (Khandaker *et al*. 2015). Although the cross section of ^{196}Au is considerable, the contribution of SHFBM, GHFBM and TGHFM level density model of ^{196}Au reaction was found to be negligibly small. The level density model conclusions are harmonious with each other up to 25 MeV. The model computations are in harmony with the experimental data in 15 MeV. The maximum calculated cross section amount of this reaction is 15 MeV.

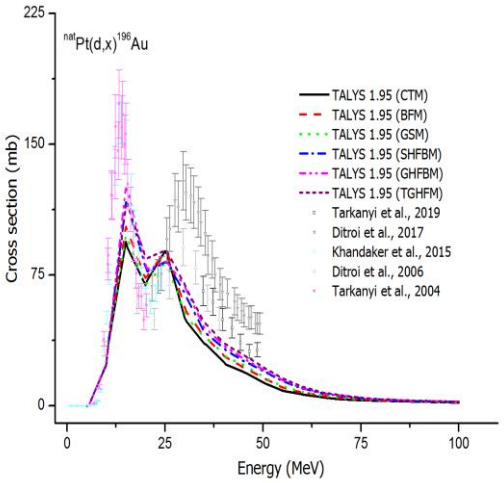

Fig. 6. Calculated cross section for $^{nat}Pt(d,x)^{196}Au$ reaction.

3.1.7 $^{nat}Pt(d,x)^{198}Au$ reaction

The relative variance analysis of production of ^{198}Au is due to the contributions from the six level density models listed in Table 1. The calculated excitation function presented in Fig. 7., is in good harmonious with the experimental data by (Khandaker *et al*. 2015) and (Ditroi *et al*. 2017) reported lower cross sections in the energy area. The level density model conclusions are harmonious with each other up to 20 MeV. The model calculations are in agreement with the experimental results in 6-30 MeV. The maximum cross section amount of this reaction is 15 MeV.

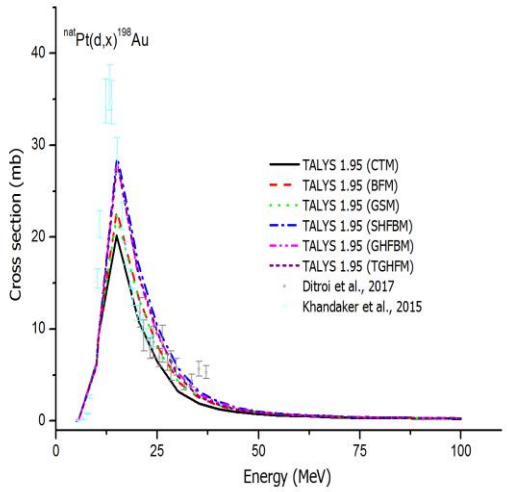

Fig. 7. Calculated cross section for $^{nat}Pt(d,x)^{198}Au$ reaction.

3.1.8 ^{nat}Pt(d,x)^{199}Au reaction

The calculated excitation function is shown in Fig. 8. together with the experimental data by (Khandaker *et al*. 2015) from EXFOR (Int Kyn. 1) library. Also, the relative variance analysis of the production of ^{199}Au radioisotope is due to the contributions from the six level density models listed in Table 1. In the 5-100 MeV energy region, the ^{199}Au radioisotope production cross section amounts are very small. The level density model conclusions are harmonious with each other up to 20 MeV. The maximum calculated cross section amount of this reaction is 15 MeV.

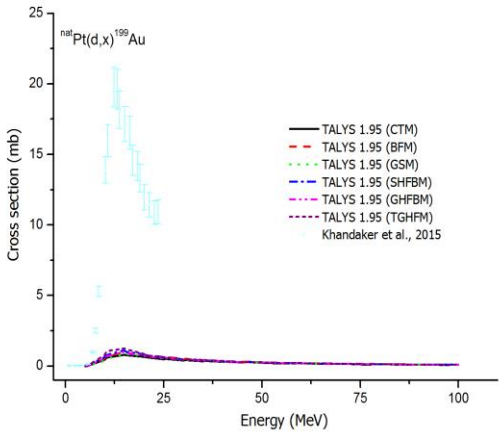

Fig. 8. Calculated cross section for ^{nat}Pt(d,x)^{199}Au reaction.

3.2. Calculations of yield for a, p, n, d, t, He-3 production

In different practical applications, information of total production activity is often more useful than microscopic cross section data. Compared to microscopic cross-sectional data; as a function of depth, bombardment energy, and target thickness, the distribution of this activity is more favorable. The product yield directly depends on the impact cross section and the compound of the target used. In this article, the theoretical yield calculations shown in Figure 9-14 are calculated using level density models for reaction products in the platinum target.

3.2.1 Alpha production

The calculated yield result with the six level density models of (d,x) reaction on ^{nat}Pt target for the production of alpha is shown in Fig. 9. In yield calculations for alpha production, level density models are close in value. The TGHFM level density model is formally different from other level density models beyond 70 MeV deuteron incident energy. In yield calculation for alpha production the maximum yield is found in the CTM level density model.

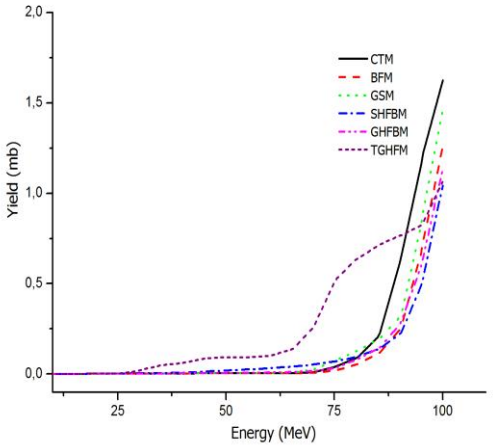

Fig. 9. Alpha production

3.2.2 Deuteron production

The calculated yield result for the production of deuteron with six level density models is shown in Fig. 10. BFM and GSM level density models have same graph, but the CTM level density model result split from the other models beyond 80 MeV deuteron incident energy and TGHFM level density model result split from the other models beyond 60 MeV deuteron event energy. In yield calculation for deuteron production the maximum yield is found in the TGHFM and SHFBM level density models.

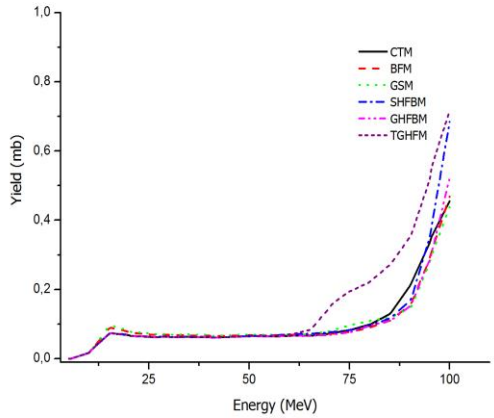

Fig. 10. Deuteron production

3.2.3 Helium-3 production

The product yield for production of Helium-3 is calculated with six level density models and is shown in Fig. 11. In the calculation of the yield for helium-3 production, the curves of all level density models resemble each other formally. The highest field calculation value for helium-3 production is observed in the CTM level density model.

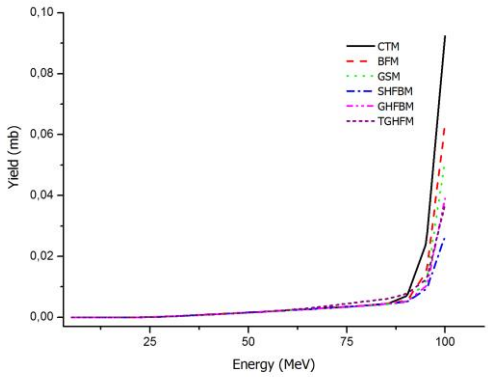

Fig. 11. Helium-3 production

3.2.4 Neutron production

The product yield for the neutron production is calculated with six level density models and is demonstrated in Fig. 12. As a yield calculation for neutron production, the curves of the six level density models examined in this article are formally similar to each other. Only the TGHFM level density model is split off as a curve from other level density models, behind 75 MeV. The highest yield calculation value for neutron production is observed in the BFM level density model at 90.5 MeV deuteron incident energy.

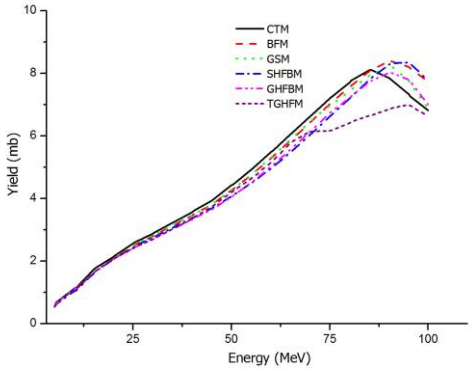

Fig. 12. Neutron production

3.2.5 Proton production

The calculated yield result with six level density models of proton production is shown in Fig. 13. When we examined the yield values calculated for proton production according to the six level density models in the yield calculation, it was observed that all the level density models were similar in shape. Only after 65 MeV, the TGHFM level density model is separated from other level density models both as a curve and as an yield value. The highest yield calculation value for proton production is observed in the GSM level density model at 100 MeV deuteron incident energy.

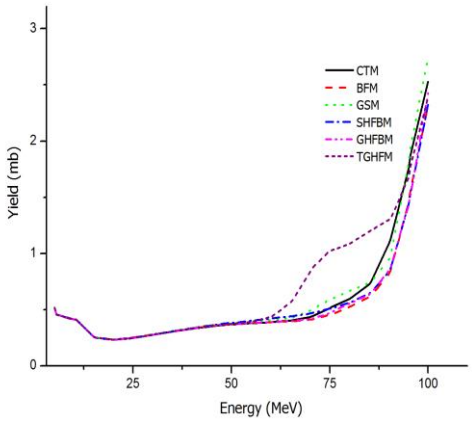

Fig. 13. Proton production

3.2.6 Triton production

The calculated yield result with six level density models on ^{nat}Pt target for the production of triton is shown in Fig. 14. In triton production yield calculation, the yield curves of SHFBM and GHFBM level density models are similar. In addition, CTM, BFM and GSM level density models are similar in their yield curves. The TGHFM level density model was calculated at a different yield value than other selective density models. In addition, the CTM, BFM, GSM level density models and SHFM and GHFBM level density models are separated from each other according to the yield value after 95 MeV deuteron incident energy. The highest yield calculation amount for triton production is observed in the TGHFM level density model at 100 MeV deuteron incident energy.

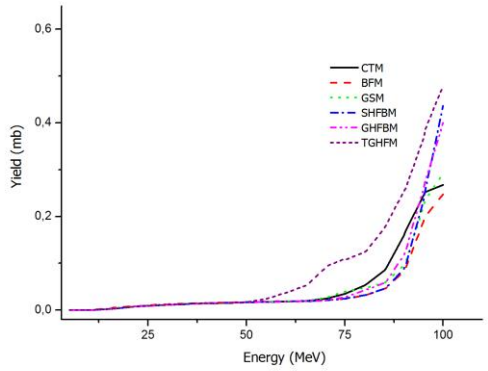

Fig. 14. Triton production

3.3. Cumulative number of levels for ^{nat}Pt(d,x)^{192,194,196,197,198}Au

The cross sections from the calculated results for the cumulative number of levels data of the ^{nat}Pt(d,x)^{192}Au reaction are shown Fig. 15. In graphical form, the cumulative number of levels values of ^{192}Au radioisotope were calculated based on the six level density models. All level density models are compatible with each other as data and curves. The calculated values for the CTM level density model are as follows; asymptotic a value: 22, 70807, shell correction: 0,24129, pairing energy: 0 and separation energy: 7.0455. While shell correction and separation energy remain at the same value for the BFM level density model; asymptotic a: 20.36875 and pairing energy value: -0.86603. In the GSM level density model, asymptotic a value is calculated as 22.27431 and pairing energy: 1.73205.

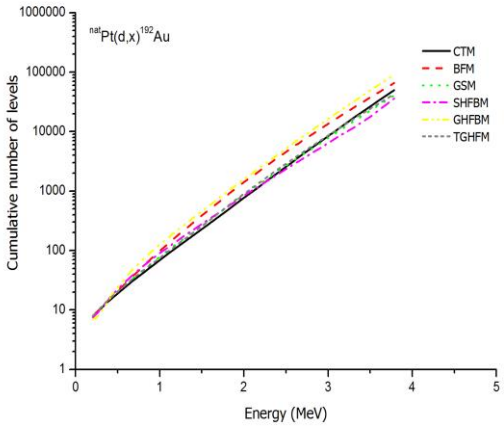

Fig. 15. Cumulative number of levels for ^{nat}Pt(d,x)^{192}Au reaction

The cross sections from the calculated results for the cumulative number of levels data of the ^{nat}Pt(d,x)^{194}Au reaction are shown Fig. 16. In graphical form, the cumulative number of levels values of ^{194}Au radioisotope were calculated based on the six level density models. All level density models are compatible with each other as data and curves. The calculated values for the CTM level density model are as follows; asymptotic a value: 22.91182, shell correction: -0.84031, pairing energy: 0 and separation energy: 6.87844. While shell correction and separation energy remain at the same value for the BFM level density model; asymptotic a: 20.55828 and pairing energy value: -0.86155. In the GSM level density model, asymptotic a value is calculated as 22.50270 and pairing energy: 1.72310.

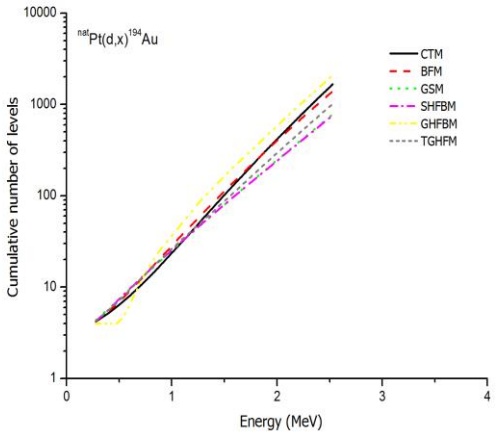

Fig. 16. Cumulative number of levels for ^{nat}Pt(d,x)^{194}Au reaction

The cross sections from the calculated results for the cumulative number of levels data of the ^{nat}Pt(d,x)^{196}Au reaction are shown Fig. 17. In graphical form, the cumulative number of levels values of ^{196}Au radioisotope were calculated based on the six level density models. All level density models are compatible with each other as data and curves. The calculated values for the CTM level density model are as follows; asymptotic a value: 23.11535, shell correction: -2.05766, pairing energy: 0 and separation energy: 6.64300. While shell correction and separation energy remain at the same value for the BFM level density model; asymptotic a: 20.74766 and pairing energy value: -0.85714. In the GSM level density model, asymptotic a value is calculated as 22.73106 and pairing energy: 1.71429.

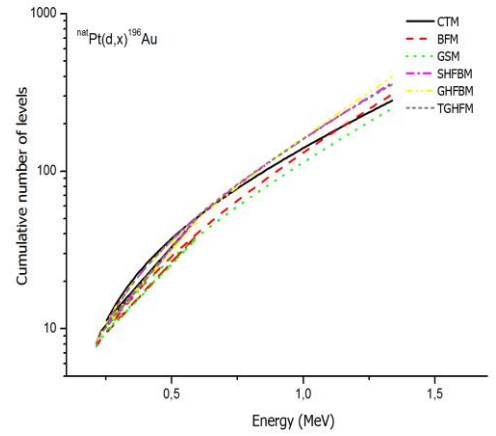

Fig. 17. Cumulative number of levels for ^{nat}Pt(d,x)^{196}Au reaction

The cross sections from the calculated results for the cumulative number of levels data of the ^{nat}Pt(d,x)^{197}Au reaction are shown Fig. 18. In graphical form, the cumulative number of levels values of ^{197}Au radioisotope were calculated based on the six level density models. All level density models are compatible with each other as data and curves. The calculated values for the CTM level density model are as follows; asymptotic a value: 23.21703, shell correction: -2.65787, pairing energy: 0.85496 and separation energy: 8.07235. While shell correction and separation energy remain at the same value for the BFM level density model; asymptotic a: 20.84229 and pairing energy value: 0. In the GSM level density model, asymptotic a value is calculated as 22.84523 and pairing energy: 0.85496.

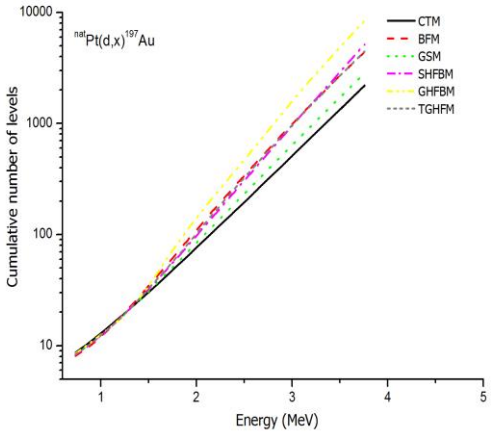

Fig. 18. Cumulative number of levels for ^{nat}Pt(d,x)^{197}Au reaction

The cross sections from the calculated results for the cumulative number of levels data of the ^{nat}Pt(d,x)^{198}Au reaction are shown Fig. 19. In graphical form, the cumulative number of levels values of ^{198}Au radioisotope were calculated based on the six level density models. All level density models are compatible with each other as data and curves. The calculated values for the CTM level density model are as follows; asymptotic a value: 23.19694, shell correction: -3.42086, pairing energy: 0 and separation energy: 6.51237. While shell correction and separation energy remain at the same value for the BFM level density model; asymptotic a: 20.35119 and pairing energy value: -0.85280. In the GSM level density model,

asymptotic a value is calculated as 16.29227 and pairing energy: 1.70561.

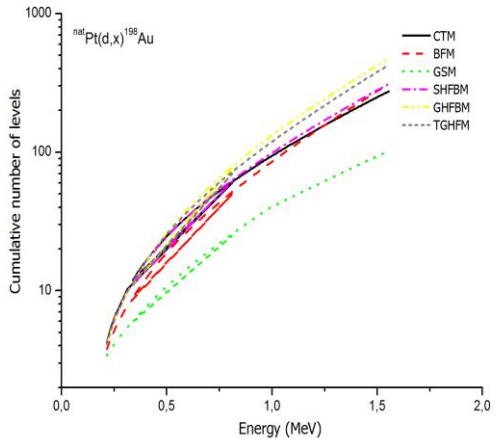

Fig. 19. Cumulative number of levels for $^{nat}Pt(d,x)^{198}Au$ reaction

4. Conclusions

In this article where I examined the effect of level density models on $^{nat}Pt(d,x)^{191-199}Au$ reaction effect sections, it was observed that SHFBM, GHFBM and TGHFM level density models could not give generally compatible conclusions with the existing experimental data in the calculated conclusions and graphs drawn accordingly. SHFBM, GHFBM and TGHFM level density models were observed to derive lower impact cross section data from experimental data on $^{nat}Pt(d,x)^{191-199}Au$ reaction effect cross-section. It is clear that CTM, BFM and GSM level density models generally give conclusions that are harmonious with existing experimental data. To specify in detail; while the CTM level density model for $^{nat}Pt(d,x)^{191,193,194,196,198}Au$ reaction, GHFBM and TGHFM models up to 28 MeV energy value for $^{nat}Pt(d,x)^{192}Au$ reaction are more compatible; after the energy value of 28 MeV the CTM level density model and SHFBM level density model can be predicted as the most compatible model for the $^{nat}Pt(d,x)^{195}Au$ reaction.

One of the most important goals of theoretical studies for nuclear reactions is to make calculations that show that reactions can be extended to energy ranges where experimental data are not available. For this purpose, in the second and third part of my study, I examined the effect of level density models on the theoretical yield and the cumulative number of levels for the $^{nat}Pt(d,x)^{192,194,196,197,198}Au$ reaction. In the calculations, I examined the effect of level density models on the theoretical yield, CTM level density model for alpha production, TGHFM and SHFBM models for deuteron production, CTM level density model for helium-3 production, BFM model for neutron production, GSM model for proton production, and TGHFM level density model for triton production show the highest yield value. When the yield calculations of the $^{nat}Pt(d,x)^{191-199}Au$ reaction are examined in figure 9-14 for alpha, deuteron, proton, neutron production, it is seen that there are generally small values.

In my calculations examining the effect of level density models for the $^{nat}Pt(d,x)^{192,194,196,197,198}Au$ reaction, it was found that all level densities except the $^{nat}Pt(d,x)^{198}Au$ reaction were compatible with each other. In the $^{nat}Pt(d,x)^{198}Au$ reaction, the GSM level density model was calculated to be separated from other models and have lower cumulative number of levels.

The data I have calculated and obtained in three different criteria based on the observation of the effects that occur in the process of performing a reaction on the basis of nuclear reactions; will be able to benefit studies aimed at developing materials to be used in different application areas, providing preliminary information to experimental and theoretical studies on nuclear reactions and creating a theoretical database. However; by examining in detail the level density states, which are a significant point in the computations of the effect section, it will contribute to the progress of theoretical models in the direction of obtaining results more compatible with experimental data.

5. References

Abdullah, A. M., Salloum, A. D., 2020. A comparison between the theoretical cross section based on the partial level density formulae calculated by the exciton model with the experimental data for ^{197}Au nucleus. *Baghdad Science Journal*, **18**, 1, 1, 139-143. doi.org/10.21123/Bsj.2021.18.1.0139.

Artun, O., 2018. Calculation of productions of PET radioisotopes via phenomenological level density models. *Radiation Physics and Chemistry*,**149**,73-83. doi.org/10.1016/j.radphyschem.2018.03.018.

Artun, O., 2019. Calculation of productions of medical ^{201}Pb, ^{198}Au, ^{186}Re, ^{111}Ag, ^{103}Pd, ^{90}Y, ^{89}Sr, ^{77}Kr, ^{77}As, ^{67}Cu, ^{64}Cu, ^{47}Sc and ^{32}P nuclei used in cancer therapy via phenomenological and microscopic level density models. *Applied Radiation and Isotopes*, **144**, 64-79. doi.org/10.1016/j.apradiso.2018.11.011.

Asres, Y. H.., Mathuthu, M., Beyene, E. Y., 2019. The study of alpha particle induced reactions on bismuth-209 isotopes using computer code COMPLET. *Journal of physics communications*, **3**,11,1-8 doi.org/10.1088/2399-6528/ab51c9.

Aydın, A., Pekdogan, H., Kaplan, A., Sarpün, İ. H., Tel, E., Demir, B., 2015. Comparison of level density models for the ^{60,61,62,64}Ni (p, n) reactions of structural fusion material nickel from threshold to 30 MeV. *Journal of Fusion Energy*, **34**(5), 1105-1108. doi: 10.1007/s10894-015-9927-2.

Bethe, H. A., 1937. Nuclear Physics B. Nuclear Dynamics, Theoretical. *Revıews of Modern Physıcs,* **9**, 2 69. doi: 10.1103/RevModPhys.9.69

Canbula, B., Bulur, R., Canbula, D., Babacan, H., 2014. A Laplace like formula for the energy dependence of the nuclear level density parameter. *Nuclear Physics A*, **929**, 54-70. doi.org/10.1016/j.nuclphysa.2014.05.020.

Canbula, B., 2020. ^{55}Mn izotopunun fotonükleer tesir kesitleri üzerinde kollektif nükleer seviye yoğunluğunun etkisi. *Süleyman Demirel Üniversitesi Fen Bilimleri Enstitüsü Dergisi*, **24**, 138-142. doi: 10.19113/sdufenbed.639828.

Dilg, W., Schantl, W., Vonach, H., Uhl, M., 1973. Level density parameters for the back-shifted fermi gas model in the mass range 40<A<250. *Nuclear Physics A*, **217**, 2, 269-298. doi.org/10.1016/0375-9474(73)90196-6.

Ditroi, F., Tarkanyi, F., Takacs, S., Hermanne, A., 2017. Extension of activation cross section data of long lived products in deuteron induced nuclear reactions on platinum up to 50 MeV. *Nuclear Instruments and Methods in Physics Research Section B: Beam Interactions with Materials and Atoms*, **401**, 56-70 doi.org/10.1016/j.nimb.2017.04.073.

Ditroi, F., Tarkanyi, F., Csikai, J., Uddin, M.S., Hagiwara, M., Baba, M., Shubin, Yu.N., Kovalev, S.F., 2006. Excitation functions of long lived products in deuteron induced nuclear reactions on platinum up to 40 MeV. *Nuclear Instruments and Methods in Physics Research B*, **243**, 1, 20-27. doi.org/10.1016/j.nimb.2005.07.206.

Ghergherehchi, M., Afarideh, H., Kim, Y.S., Park, S.Y., Lee, S.B., Shin, D.H., Chai, J.S., Mu, X.J., Lee, B.N., 2012. Dosimetry and microdosimetry of 10-220 MeV proton beams with CR-39 and their verifications by calculation of reaction cross sections using ALICE, TALYS and GEANT4 codes. *Radiation Measurements*,**47**,6,410-416. doi.org/10.1016/j.radmeas.2012.03.008.

Gilbert A; Cameron A.G.W., 1965. A composite nuclear-level density formula with shell corrections. *Canadian Journal of Physics*, **43**, (8), 1446-1496, doi:10.1139/p65-139.

Goriely, S., Tondeur, F., Pearson, J. M., 2001. A Hartree-fock nuclear mass table. *Atomic Data and Nuclear Data Tables*, **77**, 2, 311-381. doi.org/10.1006/adnd.2000.0857.

Goriely, S., Hilaire, S., Koning, A. J., 2008. Improved microscopic nuclear level densities within the Hartree-Fock-Bogoliubov plus combinatorial method. *Physical Review C*, **78**,6, 064307. doi.org/10.1103/PhysRevC.78.064307.

Hilaire, S., Girod, M., Goriely, S., Koning, A. J., 2012. Temperature-dependent combinatorial level densities with the D1M Gogny force. *Physical Review C*, **86**, 064317. doi.org/10.1103/PhysRevC.86.064317.

Hu, H., Guo, W-L., Su, J., Wang, W., Yuan, C., 2022. Implementation of residual nucleus de-excitations associated with proton decays in ^{12}C based on the GENIE generator and TALYS code. *Physics Letters B*, **831**,137183. doi.org./10.1016/j.physletb.2022.137183.

Ignatyuk, A. V., Istekov, K. K., Smirenkin, G. N., 1979. Collective effects in level density, and the probability of fission. *Yadernaya Fizika*, 0044-0027, **30**(5), 1205-1218.

Ignatyuk, A. V., Weil J. L., Raman, S., Kahane, S., 1993. Density of discrete levels in ^{116}Sn. *Physical Review C*., **47**, (4), 1504.

Kaplan, A., Özdoğan, H., Aydin, A., Tel, E. 2014. Photo-neutron cross-section calculations of ^{142,143,144,145,146,150}Nd rare-earth isotopes for

(γ,n) reaction. *Physics of Atomic Nuclei*, **77**(11), 1371-1377. doi:10.1134/S1063778814100081.

Kaplan, A., Sarpün, İ. H., Aydın, A., Tel, E., Çapalı, V., Özdoğan, H., 2015. (γ,2n)-Reaction cross-section calculations of several even-even lanthanide nuclei using different level density models. *Physics of Atomic Nuclei*, **78**(1), 53-64. doi: 10.1134/S106377881501010X.

Karpuz, N., 2016. Effect of the Level Density Parameter Ratio on the Cross Sections of Fission of Uranium Isotopes. *Acta Physica Polonica A*, **130**, 1, 306-308. doi: 10.12693/APhysPolA.130.306.

Karpuz Demir, N., 2017. Detailed Analysis of Differential Cross Sections of Elastic Scattering for n+^{208}Pb Reaction. *Acta Physica Polonica A*, **132**, 3-II, 1189-1191. doi: 10.12693/APhysPolA.132.1189.

Kavun, Y., Makwana R., 2020. Study of (γ,p) reaction cross-section calculations of ^{52}Cr, ^{54}Fe, ^{60}Ni and ^{64}Zn isotopes. *Nuclear Inst. and Methods in Physics Research B*, **472**, 72-77. doi:10.1016/j.nimb.2020.03.036.

Kavun, Y., Makwana R., 2021. Effects of some level density models and γ-ray strength functions on production cross-section calculations of ^{16,18}O and ^{24,26}Mg radioisotopes. *Journal Kerntechnik*, **86**(6), 411-418. doi:10.1515/kern-2021-1018.

Kavun, Y., Parashari S., Tel E., 2020. Investigation of (γ,p) reaction cross-section calculations of ^{40}Ca, ^{70}Ge and ^{90}Zr isotopes. *Applied Radiation and Isotopes*, **164**. doi:10.1016/j.apradiso.2020.109318.

Khandaker, M.U., Haba, H., Murakami, M., Otuka, N., Kassim, H.A., 2015. Excitation functions of deuteron-induced nuclear reactions on natural platinum up to 24 MeV. *Nuclear Instruments and Methods in Physics Research B*, **362**, 151-162. doi.org/10.1016/j.nimb.2015.09.045.

Koning, A. J., Hilaire, S., Goriely, S., 2008. Global and local level density models, *Nuclear Physics A* **810**, 13-76. doi:10.1016/j.nuclphysa.2008.06.005.

Koning, A.J., Hilaire, S., and Goriely, S., 2019. TALYS 1.95 Nuclear Research and Consultancy Group (NRG), The Netherlands.

Kulko, A. A., Skobelev, N. K., Kroha, V., Penionzhkevich, Yu. E., Mrazek, J., Burjan, V., Hons, Z., Simeckova, E., Piskor, S., Kugler, A., Demekhina, N. A., Sobolev, Yu. G., Chuvilskaya, T. V., Shirokova, A.A., and Kuterbekov, K., 2012. Excitation functions for deuterium-induced reactions on ^{194}Pt near the coulomb barrier. *Physics of Particles and Nuclei Letters*, **9**, 502, 6-7, doi:10.1134/S154747711206012x.

Lilley, J., 2018. Nükleer Fizik İlkeler ve Uygulamalar, (Çeviri Editörü: A. Aydın, İ.H. Sarpün, E. Tel ve A. Kaplan), Nobel Akademik Yayıncılık, Ankara.

Noori, S. S., Karpuz, N., Akkurt, İ., 2016. Excitation Functions of (d,n) Reactions on Some Light Nuclei. *Acta Physica Polonica A*, **129**, 1, 484-486. doi: 10.12693/APhysPolA.130.484.

Noori, S. S., Akkurt, İ., Karpuz Demir, N., 2017. Comparison of Excitation Functions of Longer and Shorter Lived Radionuclides. *Acta Physica Polonica A*, **132**, 3-II, 1186-1188. doi: 10.12693/APhysPolA.132.1186.

Noori, S. S., Akkurt, İ., Karpuz Demir, N., 2018. Excitation functions of proton induced reactions of some radioisotopes used in medicine. *Open Chemistry*, **16**, 810-816. doi: 10.1515/chem-2018-0085.

Noori, S. S., Akkurt, İ., Karpuz Demir, N., 2019. Excitation Functions for the Proton Irradiation on ^{45}Sc Target. International *Journal of Computational and Experimental Science and Engineering,* **5**, 2, 61-64. doi: 10.22399/ijcesen.547000.

Özdoğan, H., Şekerci, M., Sarpün, İ. H., Kaplan, A., 2018. Investigation of level density parameter effects on (p,n) and (p,2n) reaction cross–sections for the fusion structural materials ^{48}Ti, ^{63}Cu and ^{90}Zr. *Applied Radiation and Isotopes*, **140**, 29-34. doi.org/10.1016/j.apradiso.2018.06.013.

Sarpün, İ. H., Özdoğan, H., Taşdöven, K., Yalim, H. A., Kaplan, A., 2019. Theoretical photoneutron crosssection calculations on Osmium isotopes by Talys and Empire codes. *Modern Physics Letters A*, **34**(26),1950210. doi.org/10.1142/S0217732319502109.

Stoulos, S., Vagena, E., 2018. Indirect measurement of bremsstrahlung photons and photoneutrons cross sections of ^{204}Pb and Sb isotopes compared with TALYS simulations. *Nuclear Physics A*, **980**, 1-14. doi.org/10.1016/j.nuclphysa.2018.09.081.

Sudar, S., and Qaim, S. M., 2006. Cross sections for the formation of ^{195}Hg$_{m,g}$, ^{197}Hg$_{m,g,}$ and ^{196}Au$_{m,g}$ in α and 3He-particle induced reactions on Pt: effect of level density parameters on the calculated isomeric cross-section ratio. *Physical*

Review C, **73**(3), 034613. doi.org/10.1103/PhysRevC.73.034613.

Sziki, G.A., Simon, A., Szikszai, Z., Kerte´sz, Zs., Dobos, E., 2006. Gamma ray production cross-sections of deuteron induced nuclear reactions for light element analysis. *Nuclear Instruments and Methods in Physics Research B*, **251**, 2, 343–351. doi.org/10.1016/j.nimb.2006.07.008.

Tarkanyi, F., Takacs, S., Ditroi, F., Hermanne, A., Shubin, Yu. N., Dityuk, A. I., 2004. Activation cross sections of deuteron induced reactions on platinum. *Nuclear Instruments and Methods in Physics Research B*, **226**, 4, 490-498. doi.org/10.1016/j.nimb.2004.06.043.

Tarkanyi, F., Ditroi, F., Takacs, S., Hermanne, A., Ignatyuk, A.V., 2019. Experimental and theoretical cross section data of deuteron induced nuclear reactions on platinum. *Journal of Radioanalytical and Nuclear Chemistry*, **321**, 747. doi:10.1007/s10967-019-06624-4.

Tel, E., Akça, S., Sahan, M., Depedelen, M., Sarpün, İ.H., 2016. The comparison of (n,p), (n,α), (n,2n) and (α,n) reaction cross sections for ^{7}Li and ^{9}Be target nuclei, *Journal of Fusion Energy*, **35**(4):709-714, doi.org/10.1007/S10894-016-0094-X.

Usman, A. R., Khandaker, M. U., Haba, H., Otuka, N., Murakami, M., 2020. Production cross sections of thulium radioisotopes for alpha-particle induced reactions on holmium. *Nuclear Inst. and Methods in Physics Research B*, **469**, 42-48. doi.org/10.1016/j.nimb.2020.02.036.

Usman, A. R., Khandaker, M. U., Haba, H., Otuka, N., Murakami, M., Komori, Y., 2016. Production cross-sections of radionuclides from α-induced reactions on natural copper up to 50 MeV. *Applied Radiation and Isotopes*, **114**, 104-113. doi.org/10.1016/j.apradiso.2016.04.027.

Usman, A. R., Khandaker, M. U., Haba, H., Otuka, N., Murakami, M., 2017. Excitation functions of alpha particles induced nuclear reactions on natural titanium in the energy range of 10.4-50.2 MeV. *Nuclear Instruments and Methods in Physics Research B*, **399**, 34-47. doi.org/10.1016/j.nimb.2017.03.120.

Usman, A. R., Khandaker, M. U., Haba, H., Murakami, M., Otuka, N., 2016. Measurements of deuteron-induced reaction cross-sections on natural nickel up to 24 MeV. *Nuclear Instruments and Methods in Physics Research B*, **368**, 112-119. doi.org/10.1016/j.nimb.2015.10.077.

Yiğit, M., Tel, E., Sarpün, İ. H., 2016. Excitation function calculations for α + ^{93}Nb nuclear reactions. *Nuclear Instruments and Methods in Physics Research B,* **385**, 59–64. doi.org/10.1016/j.nimb.2016.08.019.

Yigit, M., Kara, A., 2017. Model-based predictions for nuclear excitation functions of neutron-induced reactions on $^{64,66-68}$Zn targets. *Nuclear Engineering and Technology*, **49**, 5, 996-1005. doi.org/10.1016/j.net.2017.03.006.

Vagena, E., ve Stoulos, S., 2017. Average cross section measurement for ^{162}Er (γ,n) reaction compared with theoretical calculations using TALYS. *Nuclear Physics A*, **957**, 259-273. doi.org/10.1016/j.nuclphysa.2016.09.007.

Internet references

1-http://www.nds.iaea.org/exfor/ (05.03.2022)